An imaging and systems modeling approach to fibril breakage enables prediction of amyloid behavior

Supporting Material

Wei-Feng Xue[1, 2, 3], Sheena E. Radford[2]

[1] School of Biosciences, University of Kent, Canterbury CT2 7NJ, United Kingdom
[2] Astbury Centre for Structural Molecular Biology, School of Molecular and Cellular Biology, Faculty of Biological Sciences, University of Leeds, Leeds LS2 9JT, United Kingdom
[3] Corresponding author: phone +44 1227 824821, fax +44 1227 763912, email w.f.xue@kent.ac.uk

The master equation

The master equation (Eq. 1) represents a generic ordinary differential equation system consisting of an infinite number of coupled equations, which is capable of describing the molecular mechanism of any assembly. The choice of the matrix **k** in Eq. 1, sometimes referred to as the kernel, fully determines the assembly mechanism of a system with the species distribution **c**. In Eq. 1, **c** is a column vector of N ($N \to \infty$) elements representing the species distribution in molar number concentration unit, and **k** is an operator matrix of N x N elements, i.e the kernel representing the rate constants of every possible microscopic forward or backward assembly step. The matrix **k** therefore contains detailed mechanistic information that can be used to predict the time-evolution of the species distribution **c** from any given initial distribution. By expressing the mechanism of assembly using **k**, complex assembly mechanisms can also be broken down and expressed as separate processes by expressing **k** in separate, more manageable, terms (i.e. $\mathbf{k} = \mathbf{k}_1+\mathbf{k}_2+...$) each describing a type of assembly event or an aspect of assembly. This then enables a systematic approach to resolve complex assembly mechanisms by solving Eq. 1 using experimental constraints. Hence, it is clear from Eq. 1 that the assembly mechanism of any system can be resolved through a combination of experimental and computational approaches that involve the determination of the species distribution **c** in terms of particle number concentrations (e.g. the distribution and molar concentration of amyloid fibril particles), and the separation of the mechanism into manageable terms that can be mathematically expressed and experimentally investigated individually. In the case of amyloid assembly, under the conditions without the significant parallel formation of amorphous aggregated, or other off-pathway species, **c** can be defined so that the i:th elements of **c**, c_i, correspond to the molar concentration of X_i, i.e. a particle containing i monomeric units. Using this definition of **c**, the molar concentration of monomeric units X_1 is then c_1 (the first element of **c**), and the i:th row of **k** then describes how the population of species X_i changes due to reaction to/from every other species, while the j:th column of **k** describes how species X_j leads to reactions that changes the population of every other species.

Fibril particle concentration

Assuming the total monomer equivalent protein concentration is $c_{1,tot}$ [M] in a fibril sample, then the number concentration of fibril particles in the same sample, c_F [M], is related to $c_{1,tot}$:

$$c_{1,tot} = \sum_f i_f \cdot c_F \cdot P_c(L_f)$$

Eq. S1

In Eq. S1, i_f is the number of monomers the fibril f has, and P_c is the normalized, bias-corrected fibril length distribution (1). Thus, $P_c(L_f)$ represents the population of the fibril species f with length L_f, and $c_F \cdot P_c(L_f)$ represents the particle concentration of the fibril species f. Therefore, $i_f \cdot c_F \cdot P_c(L_f)$ represents the monomer equivalent concentration of fibril species f, and summing over all species yields the total monomer equivalent concentration. The number of monomeric units the fibril species f has, i_f, can be expressed using the monomers per length ratio N_l:

$$i_f = L_f N_l$$

Eq. S2

Substituting Eq. S2 into Eq. S1 yields:

$$c_{1,tot} = c_F \cdot \sum_f L_f N_l \cdot P_c(L_f)$$
$$\Rightarrow c_F = \frac{c_{1,tot}}{\sum_f L_f N_l P_c(L_f)}$$

Eq. S3

Rearrangement then yields Eq. 2, which can be used to obtain fibril particle concentration given the total monomer equivalent concentration $c_{1,tot}$, the monomers per length ratio N_l, and the fibril length distribution P_c.

Fibril fragmentation models

To delineate the mechanism and the rates of fibril fragmentation, the process of fibril fragmentation needs be isolated from other processes, such as fibril growth. Because preformed fibril samples of β_2m under the conditions employed contain predominantly fibrils and negligible residual monomers (less than 5%, (2)), it can be assumed that fibril fragmentation is the only dominant process when such sample is perturbed mechanically. Therefore, we can assume that the matrix **k** that describes the time evolution of our experimentally measured species distribution is dominated by a fragmentation term $\mathbf{k}_{Frag}$ (i.e. $\mathbf{k} \approx \mathbf{k}_{Frag}$ under the employed experimental conditions). Assuming amyloid fibrils could break between every monomer within each fibril then the fibril fragmentation reactions (depicted in the schematic in Fig. 2a) for every possible fibril species can be described by the master equation (Eq. 1) with the following $\mathbf{k}_{Frag}$:

$$\mathbf{k_{Frag}} = \begin{bmatrix} 0 & 2k_F(2,1) & 2k_F(3,1) & 2k_F(4,1) & 2k_F(5,1) & 2k_F(6,1) & \cdots \\ 0 & \sum_{j=1}^{1} -k_F(2,j) & 2k_F(3,2) & 2k_F(4,2) & 2k_F(5,2) & 2k_F(6,2) & \cdots \\ 0 & 0 & \sum_{j=1}^{2} -k_F(3,j) & 2k_F(4,3) & 2k_F(5,3) & 2k_F(6,3) & \cdots \\ 0 & 0 & 0 & \sum_{j=1}^{3} -k_F(4,j) & 2k_F(5,4) & 2k_F(6,4) & \cdots \\ 0 & 0 & 0 & 0 & \sum_{j=1}^{4} -k_F(5,j) & 2k_F(6,5) & \cdots \\ 0 & 0 & 0 & 0 & 0 & \sum_{j=1}^{5} -k_F(6,j) & \cdots \\ \vdots & \vdots & \vdots & \vdots & \vdots & \vdots & \ddots \end{bmatrix}$$

Eq. S4

In Eq. S4, $k_F(i, j)$ describes each fragmentation models tested (Table S1). For the simplest tested case where the fragmentation rate is constant between each monomers, $k_F(i, j)$ is simply a constant:

Model 1: $k_F(i,j) = k_1$ Eq. S5

We then describe the length dependence of the fragmentation rate using a power law model function, and the position dependence using a polynomial model function to generate the following fragmentation models of increasing complexity that were tested:

Model 2: $k_F(i,j) = k_1 \cdot i^{k_2}$ Eq. S6

Model 3: $k_F(i,j) = (k_1 \cdot i^{k_2}) \cdot \left[1 + k_3 \left(\frac{j-i/2}{i/2}\right)^2\right]$ Eq. S7

Model 4: $k_F(i,j) = (k_1 \cdot i^{k_2}) \cdot \left[1 + k_3 \left(\frac{j-i/2}{i/2}\right)^2 + k_4 \left(\frac{j-i/2}{i/2}\right)^4\right]$ Eq. S8

Model 5: $k_F(i,j) = (k_1 \cdot i^{k_2}) \cdot \left[1 + k_3 \left(\frac{j-i/2}{i/2}\right)^2 + k_4 \left(\frac{j-i/2}{i/2}\right)^4 + k_5 \left(\frac{j-i/2}{i/2}\right)^6\right]$ Eq. S9

Model 6: $k_F(i,j) = \left(k_1 \cdot i^{k_2}\right) \cdot \left[1 + k_3 \left(\frac{j-\frac{i}{2}}{\frac{i}{2}}\right)^2 + k_4 \left(\frac{j-\frac{i}{2}}{\frac{i}{2}}\right)^4 + k_5 \left(\frac{j-\frac{i}{2}}{\frac{i}{2}}\right)^6 + k_6 \left(\frac{j-\frac{i}{2}}{\frac{i}{2}}\right)^8\right]$ Eq. S10

The stiff rod fragmentation model (3) tested is described by the following:

Model 7:

$$k_F(i,j) = k_1[j(i-j)]^{k_2-1}\left[\frac{(i-j)\ln j + j\ln(i-j)}{i^{k_2+1}}\right]$$ Eq. S11

In Eq. S5-S11, k_1 up to k_6 are the floating parameter to be determined quantitatively using maximum likelihood estimation method with the length distribution data obtained by AFM imaging. Only combinations that give positive k_F values are allowed in each case.

Initial seed extension kinetics

β_2m and other amyloid fibril growth is a process thought to involve a templated monomer addition reaction at growth competent sites situated at fibril ends (4–6). Since in a seeded reaction, the initial growth rate is dominated by forward growth compared with backward depolymerization or the creation of new fibril-ends by fibril fragmentation, the forward fibril monomer addition rate constants k^+ defined on a 'per fibril particle' basis can be determined from the initial slopes of normalized seeded fibril growth reaction progress traces. Assuming a forward monomer addition growth rate constants k^+ that describes the rate at which fibrils extend by monomer addition, and a backward rate constant k^- that describes the rate of fibril-end depolymerization in the absence of fibril fragmentation, then the rate of monomer depletion during fibril assembly is the following:

$$-\frac{dc_1}{dt} = k^+ c_F c_1 - k^- c_F$$ Eq. S12

Assuming seed extension reaction described in Eq. S12 and that Thioflavin T signal is linearly sensitive to protein mass in the fibril species then the change in Thioflavin T fluorescence, I_{ThT}, is proportional to the following:

$$\frac{dI_{ThT}}{dt} \propto k^+ c_F c_1 - k^- c_F$$

Eq. S13

The difference between initial Thioflavin T fluorescence, $I_{ThT,0}$, and fluorescence at monomer-fibril steady-state, $I_{ThT,ss}$, is proportional to the following:

$$I_{ThT,0} - I_{ThT,ss} \propto c_{1,t=0} - c_{1,t\to\infty}$$

Eq. S14

Combining Eq. S13 and S14, which have the same proportionality constant, yields the fluorescence signal change in normalized seed extension traces:

$$\frac{dI}{dt} = \frac{d\left(\frac{I_{ThT}}{I_{ThT,0} - I_{ThT,ss}}\right)}{dt} = \frac{k^+ c_F c_1 - k^- c_F}{c_{1,t=0} - c_{1,t\to\infty}}$$

Eq. S15

Using the fact that the monomer-fibril steady-state residual free monomer concentration is the ratio between the monomer attachment and detachment rates gives:

$$\frac{dI}{dt} = \frac{k^+ c_F c_1 - k^- c_F}{c_{1,t=0} - \frac{k^-}{k^+}}$$

Eq. S16

The initial slope at $t = 0$ is then after rearrangement:

$$\left[\frac{dI}{dt}\right]_{t=0} = \frac{k^+ c_{F,t=0} c_{1,t=0} - k^- c_{F,t=0}}{c_{1,t=0} - \frac{k^-}{k^+}} = \frac{c_{F,t=0}\left(k^+ c_{1,t=0} - k^-\right)}{\frac{1}{k^+}\left(k^+ c_{1,t=0} - k^-\right)} = k^+ c_{F,t=0}$$

Eq. S17

Thus, the second order fibril elongation rate constant can be determined in molar units on a 'per fibril particle' basis using the following:

$$\left[\frac{dI}{dt}\right]_{t=0} = k^+ c_{F,t=0}$$

Eq. S18

where the signal, I, reflects the relative fibril mass increases as function of time in normalized fibril growth reaction traces.

Generation of β_2m fibril and seed samples

All fibril formation reactions were performed in reaction buffer consisting of 10 mM monosodium phosphate and 50mM NaCl adjusted to pH 2.0 using HCl. Samples containing short fibrils used as seeds were grown from 120 μM β_2m under stirring (described in the Methods section) at 25°C for 48 h. Samples containing long-straight fibrils were prepared by seeding a freshly prepared 120 μM monomeric β_2m solution with the above short fibrils as seeds (0.1% w/w unless stated otherwise). The seeded

fibril growth reaction mixture was then incubated quiescently at 25°C for 48 hr. To create a fibril sample of distinct length distribution for validating our predictions, the new independent sample was prepared by seeding with 10% (w/w) of previously prepared fibrillar seeds, and was grown under mild agitation to facilitate a change in the initial length distribution. The fibril length distribution of this independent sample (Fig. 4 top right), therefore, was shifted to shorter lengths compared with the previous sample (compared with Fig. 1 top row), as expected for initiating elongation with a higher seed concentration under limited agitation.

Supporting References

1. Xue, W.-F., S.W. Homans, and S.E. Radford. 2009. Amyloid fibril length distribution quantified by atomic force microscopy single-particle image analysis. Protein Eng Des Sel. 22:489–96.
2. Smith, A.M., T.R. Jahn, A.E. Ashcroft, and S.E. Radford. 2006. Direct observation of oligomeric species formed in the early stages of amyloid fibril formation using electrospray ionisation mass spectrometry. J Mol Biol. 364:9–19.
3. Hill, T.L. 1983. Length dependence of rate constants for end-to-end association and dissociation of equilibrium linear aggregates. Biophys J. 44:285–8.
4. Ferrone, F. 1999. Analysis of protein aggregation kinetics. Methods Enzymol. 309:256–74.
5. Collins, S.R., A. Douglass, R.D. Vale, and J.S. Weissman. 2004. Mechanism of prion propagation: amyloid growth occurs by monomer addition. PLoS Biol. 2:e321.
6. Xue, W.-F., S.W. Homans, and S.E. Radford. 2008. Systematic analysis of nucleation-dependent polymerization reveals new insights into the mechanism of amyloid self-assembly. Proc Natl Acad Sci U S A. 105:8926–31.
7. White, H.E., J.L. Hodgkinson, T.R. Jahn, S. Cohen-Krausz, W.S. Gosal, et al. 2009. Globular tetramers of beta(2)-microglobulin assemble into elaborate amyloid fibrils. J Mol Biol. 389:48–57.

Supporting Figures

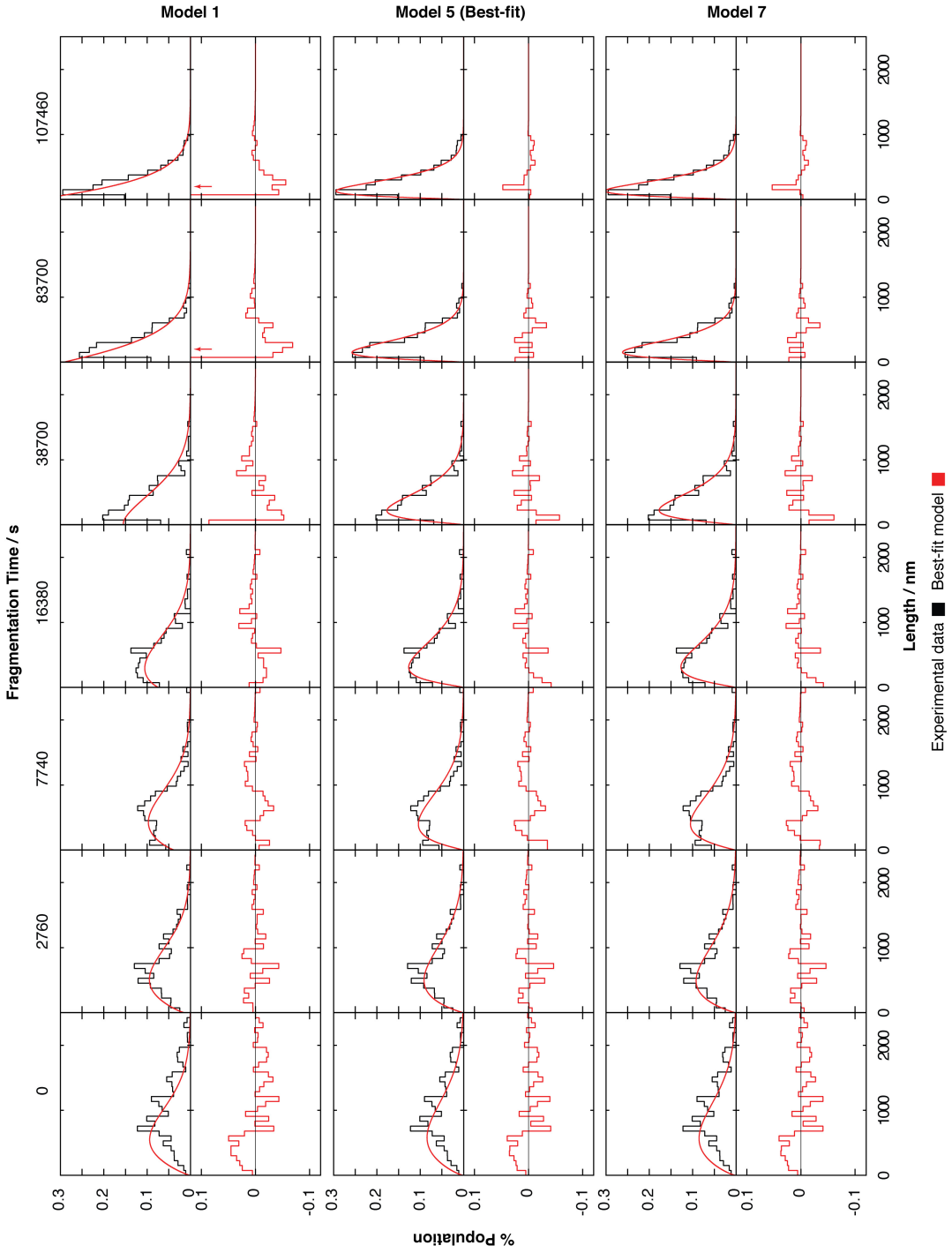

Fig. S1: Comparison between tested fragmentation models. Length distribution data of β_2m fibril fragmentation monitored by TM-AFM imaging, the same as in Fig. 1, is shown with distributions calculated from three representative models: the simplest constant fragmentation rate constant model (model 1 in Table S1), the best-fit (model 5 in Table S1), and the mechanistic Hill model for stiff rod breakage (model 7 in Table S1). The difference between each model distribution and the corresponding histogram representation of the data is show below each fitted distributions.

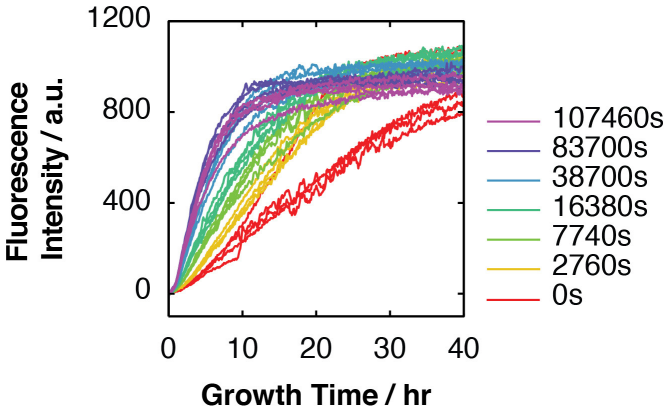

Fig. S2: Un-normalized fibril growth reaction progress curves of reactions seeded by fibril samples monitored by thioflavin T fluorescence. All four replicate reaction traces from the same experiment as the normalized traces in Fig 3a are shown. The times each sample was fragmented before addition to excess monomer to stimulate fibril growth are shown to the right.

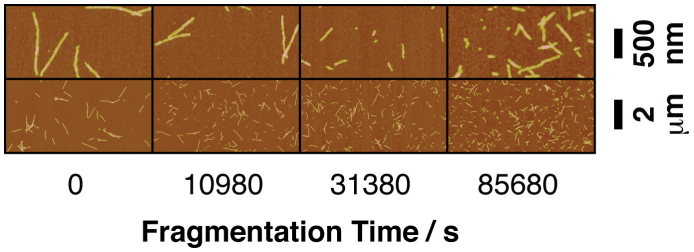

Fig. S3: Typical TM-AFM height images of the fibril samples used to validate the prediction shown in Fig. 4. The bottom row images show half (5 x 10 μm) of 1,024 x 1,024 pixel, 10 x 10 μm images. The top row images show a 4x-magnified region of the same images.

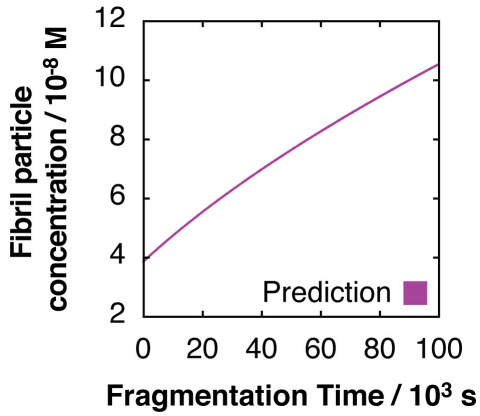

Fig. S4: Predicted increase of fibril particle concentration as fragmentation proceeds for the fibril sample undergoing fragmentation shown in Fig. 4.

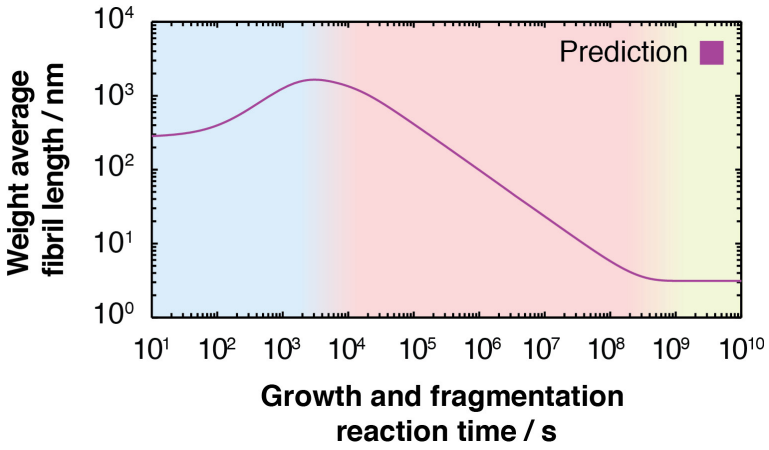

Fig. S5: Prediction of the biphasic fibril growth reaction (Fig. 6) and its behavior over extended period of time until steady-state is reached. The predicted (purple) biphasic time evolution of the weight average fibril length of a seeded fibril reaction undergoing simultaneous fibril fragmentation and fibril growth is shown on a log-log plot. The blue, red and green colored areas correspond to regions where fibril-growth dominates, fibril fragmentation dominates, and steady-state is reached, respectively. The estimated steady-state weight average particle length corresponds to fibril particles containing approximately 14 monomers based on a monomers per nm fibril length, N_l, of around 4.5 nm^{-1} (7).

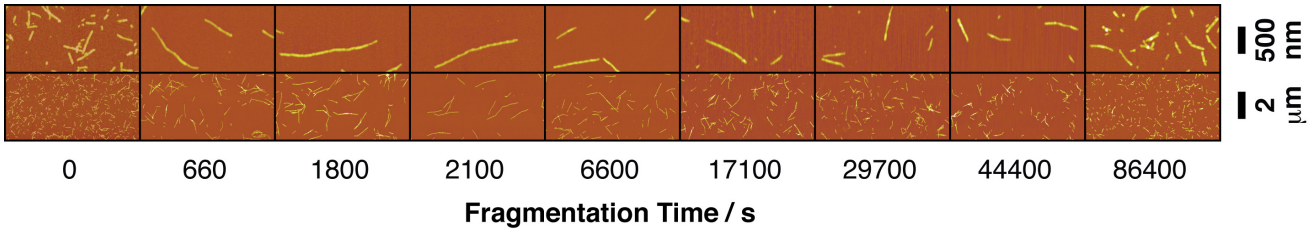

Fig. S6: Typical AFM height images of the fibril samples used to validate the prediction shown in Fig. 6. The bottom row images show half (5 x 10 µm) of 1,024 x 1,024 pixel, 10 x 10 µm images. The top row images show a 4x-magnified region of the same images.